Nonlinear ring structures in forward scattering of resonant monochromatic laser radiation

P. Jungner,* Å. Lindberg, and B. Ståhlberg
Accelerator Laboratory, Department of Physics, University of Helsinki, P.O. Box 43, FIN-00014 Helsinki, Finland
(Received 19 October 1992; revised manuscript received 12 April 1993)

We present experimental and theoretical investigations of a Gaussian laser beam interacting with Zeeman-tuned $J=1\rightarrow J=0$ atomic systems. In our experiment a single-mode cw dye-laser beam traverses a neon discharge in a longitudinal magnetic field. The excited neon transitions used for these studies are $1s_4(J=1,g=1.464)\rightarrow 2p_3(J=0)$ and $1s_2(J=1,g=1.034)\rightarrow 2p_1(J=0)$. In the laser-induced forward-scattered light, dark and bright ring-shaped structures are observed. The ring structures are investigated as a function of the magnetic detuning of the $m=\pm 1$ sublevels and as a function of the laser-beam power. We find that the line shapes of the spectra, i.e., the forward-scattered light intensities as a function of the magnetic detuning, are sensitive to the transverse intensity distribution of the laser beam. Analytical expressions based on a semiclassical theory are derived and the calculated results on the ring structures and the spectra are compared with the experimental results. Good agreement between the calculated and the experimental results are obtained only when the transverse effects are taken into account.

PACS number(s): 32.80.Bx, 33.55.Fi

I. INTRODUCTION

The propagation of electromagnetic radiation through an absorbing medium is a fundamental problem in atom and light interactions. When a beam of light propagates through a medium, the interaction processes sometimes manifest themselves as spectacular ring structures in the traversed light [1]. These phenomena can be particularly fascinating in high-intensity laser-beam penetrations through vapors and liquids. In this work we present transverse-ring-structure effects observed in a laser interaction with a magnetically tuned gaseous medium.

Since the discoveries that Hanle made [2] in the early 1920s it has been known that magneto-optic techniques are well suited for investigations of the interaction between atoms and light. Several configurations have been developed and employed in these investigations [2]. One method is based on the selective detection of only that light which is scattered in the same direction as the original exciting light propagates. During the 1960s and the early 1970s these, so-called, forward-scattering experiments were performed using conventional light sources [3,4]. These investigations founded the basic understanding and terminology of the phenomena. When lasers became available as light sources new features in the forward-scattering phenomena were observed [5,6]. Because of the high intensity of the laser beams many of the new features were caused by nonlinear interaction processes. All of these processes were not directly understood and it took many years before satisfactory theoretical descriptions were given [7–10] to explain the results of the early laser-based measurements.

Recently there has grown a renewed interest in forward-scattering and magneto-optic phenomena related to it [11–19]. Many of the investigations have dealt with the processes involved in the creation of the measured signals. Calculated signal shapes that are in agreement with the measured ones have been derived using a variety of theoretical models [10,15–21]. The mathematical treatments in some of the descriptions are very similar to those used in polarization spectroscopy. Especially forward scattering is very closely related to polarization spectroscopy [20,22]. Forward-scattering and recently the Hanle-effect studies have also attracted interest as configurations for investigations that have been extended to include partially coherent and nonmonochromatic laser light [20,23,24].

Experimentally, magneto-optical studies and, in particular, the forward-scattering studies are easy to perform. The standard procedure is to direct a linearly polarized beam of light to traverse an absorber cell. The absorber cell is in a tuneable magnetic field. The intensity of the forward-scattered light is then measured after a polarization analyzer. The transmission axis of the analyzer is oriented perpendicular to the original beam polarization. The forward-scattered light intensity is measured as a function of the magnetic field strength. This is usually done in the Faraday geometry, i.e., the magnetic field is collinear with the light beam. When the magnetic field is perpendicular to the direction of the light beam the geometry is called the Voigt geometry [12,16].

In this paper we present investigations dealing with the consequences that the transverse intensity distribution of a laser beam has on the forward-scattered light. It is well known that the transverse intensity distributions of laser beams play an important role in laser spectroscopy. Therefore it is surprising that there do not seem to exist reports on detailed studies on the effect of the spatial structure of the laser beam on forward-scattered light. Our findings show that laser beams may easily induce forward-scattered light distributions that have ring-shaped dark and bright structures. We present results on such transverse structures. Recently we have briefly reported on the first results of our studies [19]. Now we

give a more extensive description of these phenomena.

This paper is composed as follows. After this introductory section we present the experimental setup. In Sec. III we describe our theoretical treatment of the phenomena. Next we give both experimental and theoretical results on the transverse intensity distributions of the forward-scattered light. Thereafter we describe the consequences the spatial distributions have on the spectrum of forward-scattered light. We close the paper with a discussion.

II. EXPERIMENT

To study the effects that the laser-beam transverse intensity distributions create, we employ neon as the interaction matter. The neon-gas discharge cell and the devices important to this description are shown in Fig. 1. The cell has windows of high-quality fused quartz in order to minimize signal-shape degradation due to eventual birefringent and/or dichroic effects. The window separation is 9 cm and the windows are slightly tilted ($\sim 4°$) to eliminate occurrence of reflected-light interference and optical feedback effects. The inner diameter of the cell is 4 mm. The discharge current of 6 mA in the cell is maintained between a tungsten pin anode and a cylindrical stainless steel cold cathode. We focus the beam from a single-mode ring dye laser (CR-699-21) into the center of the discharge. To ensure that the laser beam is linearly polarized, we have introduced a high-quality prism polarizer in the entrance beam. In the outgoing beam we have another high-quality crossed prism polarizer to serve as an analyzer. As detectors we employ (depending on the measurements) either a 1728 pixel charge-coupled device (CCD) or an ordinary *p-i-n* photodiode. The CCD type is TH7811CD (Thomson Composants Militaires et Spatiaux) and it has the pixel size of 13×13 μm^2. The forward-scattered light intensity can be so high that it is clearly seen by the bare eye for nonzero magnetic fields. For high forward-scattered light intensities we introduce a neutral density filter (neutral density equal to 1.0) in order to avoid saturation of the detectors. The longitudinal magnetic field is derived from a pair of Helmholtz coils. The coils have a radius of 5 cm which is slightly larger than the useful interaction length (4 cm) of the discharge. The field uniformity over the useful discharge has been measured to be better than 1%. The measurement of the field uniformity has been carried out using two Teslameters, the analog scales of which allow a reading accuracy within 1%. Hall-effect probes have been shifted over the useful discharge volume with a positioning device constructed for the purpose.

In our measurements we determine the Doppler-broadened line center of the investigated transition in the following way. After wavemeter diagnostics (to find the transition wavelength) we attenuate the laser beam to a sufficiently low intensity. We monitor the absorption of the traversed beam and tune the laser frequency until maximum absorption is reached. The ring dye laser is optimized to lase on a TEM_{00} mode. Thus a Gaussian transverse intensity distribution is introduced into the neon cell. In Fig. 2 a recording of the laser-beam transverse profile is shown. The recording has been taken after the beam has traversed the absorber cell without a discharge. A suitable intensity on the CCD array has been adjusted by tuning the analyzer slightly from its crossed orientation. The spikes seen in the recording of Fig. 2 arise mainly from interference effects in the protective plastic layer on the CCD surface. In our recordings we have tried to minimize the spiky structure by adjustments of the CCD orientation. The recording of Fig. 2 is a representative one and the beam profile it shows is the one used in the measurements. The triangular points in Fig. 2 are from a least-squares fit of a Gaussian function to the experimental data.

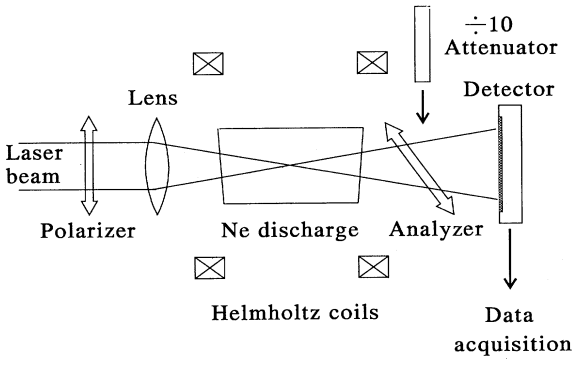

FIG. 1. Schematics of the experiment. The attenuator is inserted in measurements that saturate the detector. The detector is a CCD for measurements of forward-scattered light distributions. For measurements of forward-scattering spectra the detector is a *p-i-n* diode.

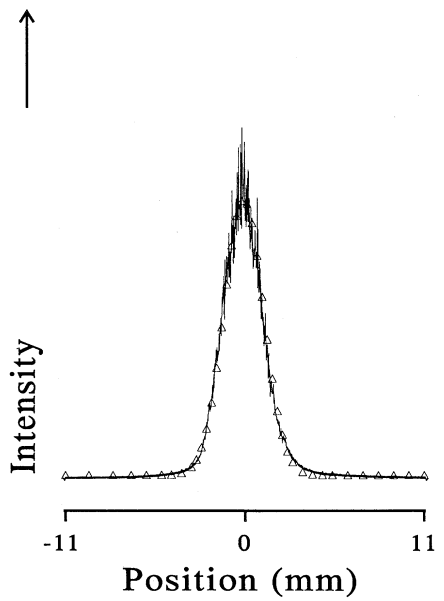

FIG. 2. The transverse intensity distribution of the interacting laser beam; the beam intensity as a function of the position on the CCD. The triangles are from a least-squares fit of a Gaussian function to the recorded curve.

III. THEORY

We have previously published papers on our theoretical treatment concerning these types of magneto-optical effects [17–19,25,26]. There are also other theoretical investigations focused on the same problems, but in those works [7–11,15,20] different approaches compared to ours have been chosen. In the following we outline our semiclassical calculations in order to make the present description comprehensible.

A representation that describes the monochromatic laser field at the entrance of the absorber is

$$\mathbf{E}_{\text{in}}=\hat{\boldsymbol{\epsilon}}E\exp[i(kz+\omega t)]+\text{c.c.}\ , \tag{1}$$

where $\hat{\boldsymbol{\epsilon}}$ is the unit vector of the beam polarization. The polarization that the electric field induces is of the form

$$\mathbf{P}=\mathcal{P}\exp[-i(kz+\omega t)]+\text{c.c.} \tag{2}$$

and the electric field in the medium is of the form

$$\mathbf{E}_m=\mathcal{E}\exp[i(kz+\omega t)]+\text{c.c.} \tag{3}$$

The amplitudes in Eqs. (1)–(3) are assumed to be slowly varying. Substitution of Eqs. (2) and (3) into the wave equation yields, after integration,

$$\mathcal{E}^*(z)=\hat{\boldsymbol{\epsilon}}^*E^*-\frac{i\omega}{2c\varepsilon_0}\int_0^z\mathcal{P}(\mathbf{E}_m(z'))dz'\ . \tag{4}$$

As the sample is considered to be optically thin we have $\mathcal{P}(\mathbf{E}_m(z))\simeq\mathcal{P}(E_m(z=0))$. The field out from the cell is

$$\mathbf{E}_{\text{out}}=\mathbf{E}_{\text{in}}+\frac{\omega L}{c\varepsilon_0}\text{Im}\{\mathcal{P}\exp[-i(kz+\omega t)]\}\ , \tag{5}$$

where L is the length of the interacting medium.

Insertion of an analyzer in the beam is modeled by a projection operator, i.e., a unit vector $\boldsymbol{\alpha}$ parallel with the analyzer transmission axis. For an arbitrary analyzer angle the measured signal becomes proportional to

$$(\mathbf{E}_{\text{out}}\cdot\boldsymbol{\alpha})^2=(\mathbf{E}_{\text{in}}\cdot\boldsymbol{\alpha})^2+2(\mathbf{E}_{\text{in}}\cdot\boldsymbol{\alpha})\frac{\omega L}{c\varepsilon_0}\text{Im}\{\boldsymbol{\alpha}\cdot\mathcal{P}\exp[-i(kz+\omega t)]\}+\left[\frac{\omega L}{c\varepsilon_0}\text{Im}\{\boldsymbol{\alpha}\cdot\mathcal{P}\exp[-i(kz+\omega t)]\}\right]^2\ . \tag{6}$$

In the forward-scattering case $\boldsymbol{\alpha}$ is perpendicular to $\mathbf{E}_{\text{in}}$ and only the third term in Eq. (6) remains. For discussion of the role of the two other terms we refer to our previous publications [25,26].

The times associated with the optical frequencies are very short compared with the measurement time constants. Time averaging gives the signal

$$S\propto[\text{Im}(\boldsymbol{\alpha}\cdot\mathcal{P})]^2\ . \tag{7}$$

In the present forward-scattering case the signal contains only the parts of the induced polarization responsible for the dispersion of the medium. The polarization is calculated to the third order using density-matrix formalism [27]. A pure $J=1$ to 0 transition is considered (Fig. 3). The linearly polarized electric field imposes the magnetic sublevel coupling selection rule $|\Delta m|=1$. As the investigations are restricted to low beam intensities the calculation of the signal is carried out as an expansion series of the laser intensity up to the second order. The laser frequency is assumed to be tuned to the absorber line center. In the Doppler limit the signal is

$$S=[W(\Delta)]\left[-\frac{2\Delta}{\sqrt{\pi}ku}+\beta^2\left[\frac{2\gamma_{ab}-\gamma_a-\gamma_b}{\gamma_a(2\gamma_{ab}-\gamma_b)}\frac{\Delta}{\gamma_{ab}^2+\Delta^2}+\frac{2}{2\gamma_{ab}-\gamma_b}\frac{2\Delta}{\gamma_b^2+4\Delta^2}\right]\right]^2, \tag{8}$$

where $\Delta=g\mu_B B/h$ is the magnetic splitting between the Zeeman sublevels (Fig. 3) and ku is the Doppler linewidth. The population damping constant of the upper (lower) level is denoted by γ_a (γ_b) and the coherence damping constant by γ_{ab}. The broader dispersive part associated with γ_{ab} arises from the population transfer (the population effect [25,26]) between the levels a and b. The narrower dispersive part associated with γ_b originates from the coherent Hanle signal (the Zeeman coherence effect [25,26]).

The factor β in Eq. (8) is the Rabi frequency ($\beta=E\mu/h$). A fundamental (TEM_{00}) laser mode requires introduction of a spatially dependent Rabi frequency

$$\beta^2(r)=\left[\frac{E_0\mu}{h}\right]^2\exp\left[-\left[\frac{r}{r_0}\right]^2\right], \tag{9}$$

where r_0 is the distance from the beam center where the intensity has decreased to $1/e$ of its maximum value $(E_0)^2$. The factor $W(\Delta)$ in Eq. (8) is due to the Doppler

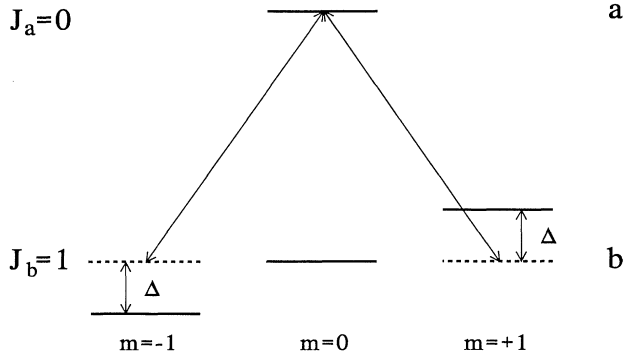

FIG. 3. The level system considered. A magnetic field detuning Δ shifts the sublevels $m=+1$ and -1 from the laser-field interaction between the levels a and b.

background and it is proportional to the laser intensity

$$W(\Delta,r)=\text{const}\times\left[\frac{\beta(r)}{ku}\right]^2\left\{\exp\left[-\left[\frac{\Delta}{ku}\right]^2\right]\right\}. \quad (10)$$

It should be pointed out that in deriving Eq. (8) we have not included any variations of the laser beam in the z direction. As we focus the beam into the cell the nonlinear contributions change with the size of the beam. Strictly taken this should also be taken into account. This effect is, however, smaller than those induced by the transversal intensity distribution of the beam and in order to keep our model simple we do not consider z direction effects.

The features of forward-scattering signals as a function of the magnetic detuning Δ have been studied many times before [6,10,17,18]. The purpose of this work is to compare the spatial structures predicted by Eqs. (8)–(10) with experimental recordings and to investigate how the signals as a function of the detuning Δ depend on the spatial structure.

IV. RESULTS ON TRANSVERSE LIGHT INTENSITY DISTRIBUTIONS

In this section we present both experimental and calculated results. First we show how the transverse intensity distribution of forward-scattered light depends on the magnetic field detuning. Next we show how it depends on the laser-beam power.

All experimental recordings shown in this paper have been taken with a lens at the cell entrance having a focal length $f=10$ cm. We have examined the scattered light intensity distributions using other lenses having $f=100$, 50, and 30 cm. Small changes in the distributions can be observed with different lenses. However, the relevant features of the distributions remain quite insensitive to the selection of the lens focal length.

Figure 4 shows the forward-scattered light intensity as a function of the position on the CCD. To scan all the CCD pixels we have used a time of 1 s. The recordings have been obtained using the $1s_4(J=1,g=1.464)$-$2p_3(J=0)$ transition in neon. The corresponding laser wavelength is 607.4 nm. All the recordings shown in Fig. 4 have been obtained with the laser input power 10 mW and the gas pressure 75 Pa (0.56 Torr). The magnetic field detuning ($\Delta=g\mu_B B/h$) starts from 37 MHz and ends with 333 MHz. For low magnetic detunings the forward-scattered light intensity distribution resembles the shape of the Gaussian input laser beam. Very obvious transverse structures appear for magnetic field detunings between 130 and 250 MHz while they disappear again for detunings above 300 MHz. If the transverse structures are viewed in two dimensions (i.e., viewed on a piece of paper) the dips in the recordings of Fig. 4 constitute to dark rings. The intensity maxima in Fig. 4 form bright rings or a bright spot in the center of the scattered light. The structures are very stable. For the 10-mW input power and a detuning $\Delta=260$ MHz the total scattered light power is 0.3 mW.

A calculated reproduction of the curves presented in Fig. 4 can be done using Eqs. (8)–(10). The results are plotted in Fig. 5. For the decay parameters (in frequency units) we have used $\gamma_a=10$ MHz, $\gamma_b=30$ MHz, $\gamma_{ab}=84$ MHz. We have scaled Eqs. (8) and (10) so that $ku=1$.

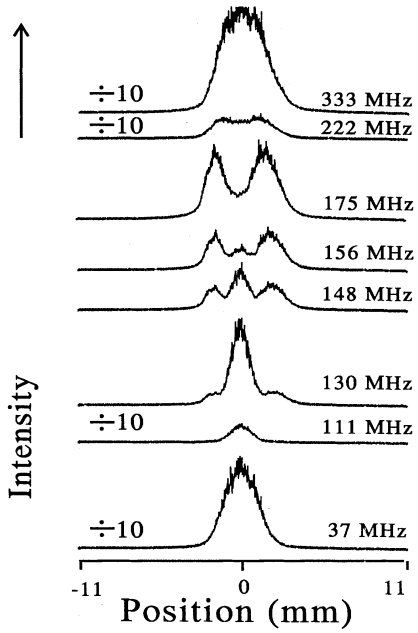

FIG. 4. Experimental results on the forward-scattered light intensity as a function of the position on the CCD. Neon transition: $1s_4(J=1,g=1.464)$-$2p_3(J=0)$. The magnetic detuning parameter starts from $\Delta=37$ MHz and ends with $\Delta=333$ MHz. All the recordings have been obtained using the constant laser power of 10 mW. The recordings where ten times attenuation of the scattered light has been required are denoted by ÷10.

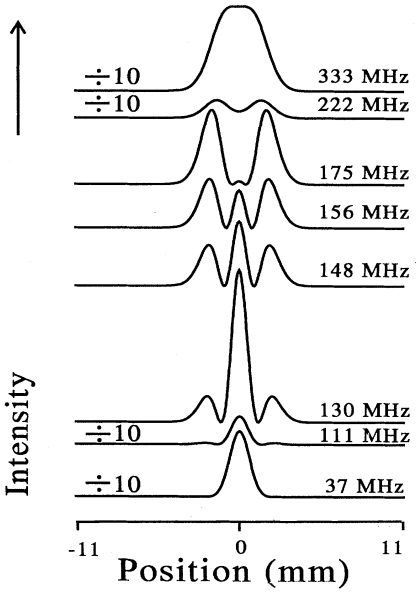

FIG. 5. Calculated results on the transverse intensity distribution of forward-scattered light to be compared with the curves of Fig. 4. The curves have been calculated using Eqs. (8)–(10).

The Rabi frequency used is $\beta^2=0.45$ MHz^2. This represents an average Rabi frequency value since we have not taken into account the size change of the beam due to the focusing in the experimental procedure. The consistency of our choice of the decay parameters γ_b and γ_{ab} has briefly been checked against data obtained from zero-field level-crossing experiments similar to those in Ref. [25]. Fixing the values for the decay parameters we have searched for a β^2 value which produces curves that resemble the experimental ones. The beam radius r_0 has been extracted from the least-squares fit of Fig. 2 resulting in $r_0=1.7$ mm. We have not tried to perform detailed fit procedures of our theoretical expressions to the experimental data. We have only inserted realistic parameter values into our equations to examine if the relevant features of the experimental curves can theoretically be reproduced.

The explanation for the structures is as follows. The laser power is kept constant at a level where the nonlinear contributions (i.e., the population effect and the Zeeman coherence effect) are significant. For small magnetic detunings (Δ) the nonlinear parts in Eq. (8) are dominant and the transverse intensity distribution is nearly Gaussian. Because the nonlinear parts have a $\beta^4(r)$ dependence the width of the light distribution for low Δ:s is narrower than that of the original incoming beam. For intermediate Δ:s the linear part (which is of an opposite sign) becomes comparable to the nonlinear parts. Thus, for some intensity, i.e., for some value of $\beta(r)$ the linear and the nonlinear parts will cancel and cause a dip in the transverse intensity distribution. For large magnetic detunings (Δ) the nonlinear parts are tuned out of interaction and only the linear part remains. The intensity distribution becomes Gaussian again. The linear part is proportional to $\beta^2(r)$ which results in a broader distribution than that caused by the nonlinear parts.

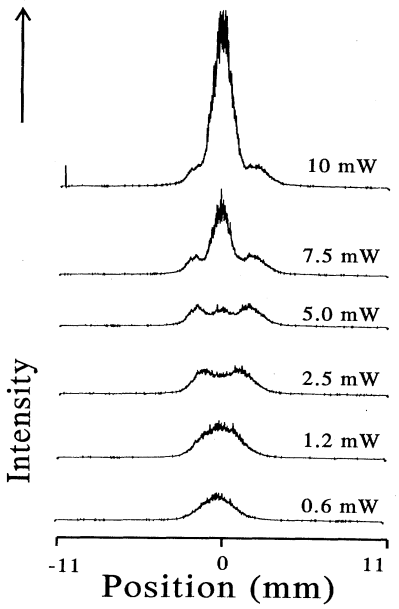

FIG. 6. Experimental forward-scattered light intensity as a function of the position on the CCD. Neon transition: $1s_4(J=1,g=1.464)$-$2p_3(J=0)$. To the right the total laser-beam power into the cell is given starting from 0.6 mW and ending with 10 mW. All curves have been recorded with the constant magnetic detuning $\Delta=130$ MHz.

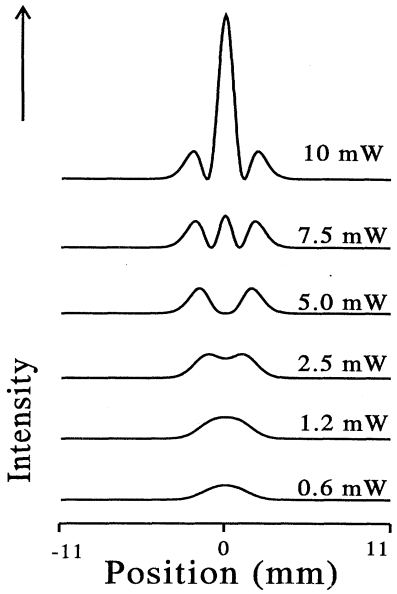

FIG. 7. Calculated results to be compared with the experimental ones of Fig. 6. The curves have been calculated using Eqs. (8)–(10).

To check the validity of the explanation given above it is straightforward to study the distributions as a function of the laser power. In Fig. 6 recordings of the transverse intensity distribution for various laser powers are shown when the magnetic detuning has been kept at the constant value $\Delta=130$ MHz. The same kind of structures as those presented before appear. These are again reproduced using Eqs. (8)–(10). The calculated results are shown in Fig. 7. Obviously for low laser powers the linear part of Eq. (8) is dominant while the nonlinear parts become dominant for high laser powers. The agreement between the experimental recordings and the calculated curves is good up to the beam power of about 10 mW. For higher powers the theory predicts much higher signals than that actually recorded. One reason for this discrepancy between the experimental results and the theoretical predictions is that Eq. (8) is derived in a low power approximation.

V. CONSEQUENCES TO SPECTRA OF FORWARD-SCATTERED LIGHT

It has already been mentioned that usually in these experiments the intensity of the forward-scattered light is measured as a function of the magnetic field detuning. In some cases the scattered light intensity is high enough to be easily measured using an ordinary photodiode. Some experiments require a photomultiplier to serve as a detec-

tor. Depending on the amount of the scattered light that is measured, i.e., the part that is integrated, the spectrum shape is altered.

In Fig. 8 two experimental recordings are shown. Both curves have been recorded using the $1s_4(J=1,g=1.464)$-$2p_3(J=0)$ neon transition. The laser input power to the cell was 7 mW, the gas pressure was 75 Pa, and the discharge current was 6 mA. The upper curve has been measured with a small active area photodiode placed in the center of the scattered light. The diode active surface area is approximately 1×1 mm^2 while the diameter of the visible scattered light distribution was around 2 cm. Thus the upper curve constitutes to a recording of a quite constant beam intensity over the observed area. Or, in other words, the upper curve represents a case where a low degree of integration of the scattered light has been used. The lower curve in Fig. 8 represents a case where a high degree of integration of the scattered light has been used. In recording of the lower curve a lens was inserted after the analyzer in order to collect the scattered light on the photodiode. Approximately 50–70 % of the total scattered light was detected by the photodiode. For the 7-mW input power to the cell the scattered light power was 0.2 mW for the detuning $\Delta=260$ MHz. The measurement time for one curve of those in Fig. 8 was around one to two minutes.

The most distinguishable difference in the two recordings of Fig. 8 can be seen in the nonlinear contributions in the vicinity to the zero-detuning values in the curves.

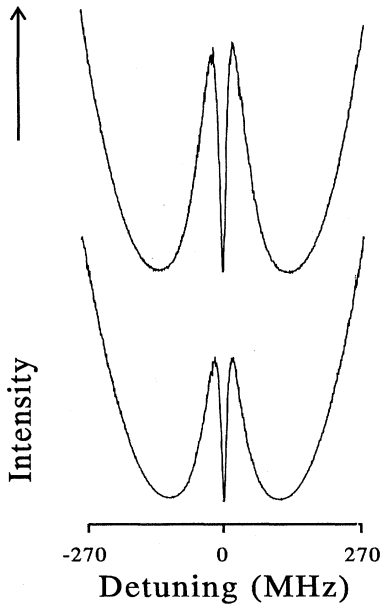

FIG. 8. Experimental forward-scattering spectra; the scattered light intensity as a function of the magnetic detuning Δ. Recordings obtained using the neon transition $1s_4(J=1,g=1.464)$-$2p_3(J=0)$ and the laser power 7 mW. In the upper curve only the light in the very center of the forward-scattered distribution is recorded. The lower curve corresponds to a recording where most of the forward-scattered light is collected (by a lens) on the detector. For the detuning $\Delta=260$ MHz the scattered-light power is 0.2 mW.

The upper curve shows—as it should—a more pronounced structure compared with the lower one. The light intensity in the beam center is higher than the average (integrated) intensity. A more careful examination—particularly an expanded vertical axis of Fig. 8—shows another difference between the curves. The minima on both sides of the zero-detuning value in the upper curve reach well the same intensity value as the dip in the center. In the lower curve the side minima are slightly above the intensity value of the center dip. This second feature in forward-scattering spectra is better observed for transitions having larger level linewidths.

In Fig. 9 two experimental recordings are shown where the $1s_2(J=1,g=1.034)$-$2p_1(J=0)$ neon transition has been used. This transition wavelength is 585.2 nm. The laser power was 8 mW, the neon-gas pressure was 75 Pa, and the discharge current 6 mA. Again as in the previous figure the upper curve in Fig. 9 has been recorded with the photodiode in the center of the scattered-light distribution while the lower curve has been obtained by focusing 50–70 % of the scattered light on the photodiode. Also, again as in the previous figure the nonlinear contribution in the central parts of the curves in Fig. 9 is more pronounced for the upper "nonintegrated" case than for the lower "integrated" case. Moreover, now the wing structure difference between the two cases is much more clear. The upper "nonintegrated" recording shows wing minima extending much closer to the center dip value than those of the lower "integrated" recording. It is also clear that the wing minima in the "nonintegrated" upper curve do not fully reach the center dip value in this case of the $1s_2$-$2p_1$ transition.

In comparing the recordings of Fig. 9 with those of

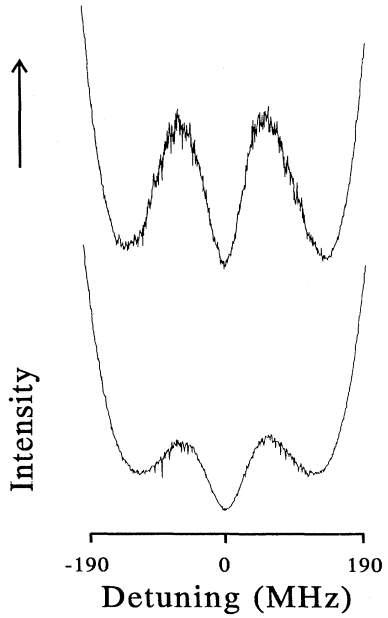

FIG. 9. Experimental forward-scattering spectra. Neon transition: $1s_2(J=1,g=1.034)$-$2p_1(J=0)$. Laser power 8 mW. For the detuning $\Delta=180$ MHz the scattered-light power is 8 μW. Otherwise the same as Fig. 8.

Fig. 8 it is obvious that those of Fig. 9 show more noise than the ones in Fig. 9. The transition $1s_2$-$2p_1$ (Fig. 9) is much more absorptive than the transition $1s_4$-$2p_3$ (Fig. 8). For the 8-mW input power to the cell (Fig. 9), the total scattered-light power was around 8 μW for the detuning $\Delta = 180$ MHz. In principle, by using a smaller active area photodiode than the (1×1 mm^2) one used in this work, we would reduce the spatial integration. A smaller detector would, however, require a longer measurement (integration) time and/or effective filtering to improve the signal to noise ratio in the case of the absorptive transition $1s_2$-$2p_1$ (see upper curve of Fig. 9).

Next we present our calculated results. In Fig. 10 two curves are shown to be compared with those of Fig. 8 and, particularly, with those of Fig. 9. The upper curve of Fig. 10 constitutes the "nonintegrated" case and it has been obtained using Eqs. (8) and (10) without any assumptions on the transverse intensity distribution on the interacting beam. To obtain the lower curve Eq. (9) has been used in combination with Eqs. (8) and (10) together with an integration over r. The damping constants used in calculating both curves are (in frequency units) $\gamma_a = 15$ MHz, $\gamma_b = 75$ MHz, and $\gamma_{ab} = 110$ MHz. The peak value for the Rabi frequency used is $\beta^2 = 0.5$ MHz^2. Again, as before, we have not carried out a detailed fit to obtain these parameters. However, it should be mentioned that calculated forward-scattering signal shapes are sensitive to the damping constant and Rabi frequency values. Comparison of the two curves in Fig. 10 shows the same features as the experimental ones of Fig. 8 and even more as those of Fig. 9. Our calculations show that in the "integrated" case the wing minima deviations from the center dip value are more pronounced for larger damping constant values than for smaller ones.

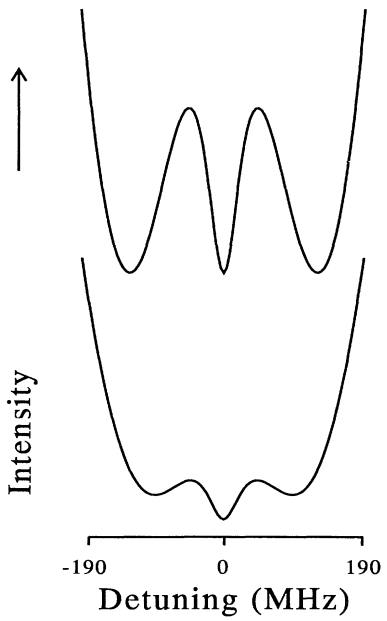

FIG. 10. Calculated forward-scattering spectra to be compared with the experimental ones of Fig. 9. Calculations performed using Eqs. (8)–(10).

VI. DISCUSSION

We have investigated the transverse intensity distribution of forward-scattered light induced by a Gaussian laser beam. In the first part concerning the results in this work we have compared experimental and calculated forward-scattered light intensity distributions. In Figs. 4 and 5 we have presented this comparison when the magnetic sublevel detuning has been varied. In Figs. 6 and 7 we have presented the results when the laser power has been varied. The experimental curves of Figs. 4 and 6 have been recorded using the $1s_4(J=1)$-$2p_3(J=0)$ neon transition. The conclusion from the results of Figs. 4–7 is that the agreement between our experimental and calculated results is satisfactory.

In the second part concerning the results in this work we have presented forward-scattering signals as a function of the magnetic detuning. We have presented experimental results in Figs. 8 and 9 obtained with the neon transitions $1s_4(J=1)$-$2p_3(J=0)$ and $1s_2(J=1)$-$2p_1(J=0)$, respectively. In Fig. 10 we have presented the calculated results. Comparing the curves of Figs. 8–10, it can be concluded that if accurate values are extracted from fit procedures of theoretical expressions to experimental data, it is worthwhile to consider taking into account the transverse effects in the light and matter interactions.

Concerning comparison of the experimental results of Fig. 9 with the calculated ones of Fig. 10, a more detailed discussion is required. As already mentioned, the neon transition $1s_2(J=1)$-$2p_1(J=0)$ is a very absorptive one. For instance, with this transition it is hard to obtain any results by removing the analyzing polarization prism from our experiment in order to carry out a conventional zero-field level-crossing experiment, i.e., by measuring the signal directly from the beam that has traversed the sample [25]. By using the forward-scattering method ("where only the light that has interacted is detected") results are easily obtained. However, these results do not fully agree with our calculated ones. The calculated upper curve of Fig. 10, representing the "nonintegrated" case, shows a signal structure where the wing minima extend exactly to the same minimum value as the center one. For the experimental upper curve of Fig. 9 this is not the case. One reason for this discrepancy between the experimental and calculated results is due to the following. In deriving Eqs. (8)–(10) we assumed an optically thin matter. Neon cannot be considered optically thin when we are dealing with the $1s_2(J=1)$-$2p_1(J=0)$ transition. However, as the curves of Figs. 9 and 10 show, a considerably better agreement between experimental and theoretical results is obtained by including the transverse effects in the description.

In working with the $1s_2(J=1)$-$2p_1(J=0)$ transition we have studied the optical depth problem by lowering the gas pressure from the value 75 Pa. We can lower the pressure to 30–40 Pa and for a rapid experiment even down to around 10 Pa. For the pressures 30–40 Pa we cannot observe relevant changes in the signals compared with those we observe at 75 Pa. Below 30 Pa the sputtering from the cell cathode becomes very effective and the

discharge conditions are degraded so fast that the signal shapes change during a recording.

This work has dealt with the problem of the wing minima appearance in forward-scattering spectra. At this point, a comparison to one phenomenon capable of producing line shapes similar to those reported here should be mentioned. If the interacting electromagnetic field is allowed to be partially coherent the wing minima in forward-scattering spectra do not reach the zero-detuning value [20]. The theoretical spectra [20] resemble very much those we have presented. We believe, however, that particularly in our experiment the line shapes are due to the transverse effects and that they are much more significant than those of fluctuating fields. Usually effects due to fluctuations in a laser field become observable when the spectral width of the laser is comparable to the linewidths in the experiment. In our case the linewidth of our laser is around 500 kHz while the experiment response linewidths are tens of MHz.

A comment, worth mentioning, originates from a closer look at the experimental recordings of Figs. 8 and 9. Obviously the curves show slight asymmetries, i.e., they are not exactly similar to each other on both sides of the zero-detuning value. Symmetries of forward-scattering spectra are extremely sensitive to the polarization properties of the interacting field and to the mutual orientation of the polarizer and the analyzer prisms. Very small deviations from a perfect perpendicular orientation of these prisms show up as asymmetries in the spectra.

To perform forward-scattering experiments using neon as the sample is quite ideal. Neon provides transitions with pure $J=1$-$J=0$ states. Natural neon consists of approximately 91% of ^{20}Ne, 9% of ^{22}Ne, and a vanishing amount of ^{21}Ne. Thus, in analyzing results from neon experiments, usually there are no problems with hyperfine structures and the experimental results can be compared with not too complicated theoretical predictions. However, due to the two even neon isotopes, some features in forward-scattering spectra can be expected which have not been included in this work.

In this work we have investigated the case where the single-mode laser frequency has been assumed to be perfectly tuned to the center of an absorber velocity profile. The velocity profile has been assumed to consist of only a single Gaussian-shaped distribution. Because the isotope shifts of ^{20}Ne and ^{22}Ne transitions are nearly the same [28,29] as the velocity profile linewidths for the transitions, the actual absorbing profile consists of two overlapping velocity profiles. Our preliminary experimental results show that the line shapes of forward-scattering spectra also depend on the detuning of the laser frequency from the absorber line center. In the case of two overlapping profiles the laser frequency is always detuned from one of the centers of the two distributions. To take into account the consequences to the spectra because of the laser frequency detuning from the two absorber line centers requires a more laborious theoretical calculation than the one considered in this publication. Work on the dark and bright ring structures and the spectra dependencies on the laser frequency detuning from absorber line centers is in progress.

Finally we compare our ring structures with those of, so-called, cone or conical emission. Recently conical emission has been studied quite thoroughly [30–33]. Conical emission can be induced with both pulsed and cw lasers. A clear difference to our forward-scattering experiment is that conical emission is typically produced with several hundred milliwatts of cw power or pulsed power from watts up to kilowatts. A conclusion that can be drawn from this is that much higher-order nonlinearities are induced in the conical emission case than in our forward-scattering case. Another difference between these cases is that in conical emission the laser frequencies are typically detuned well away (usually blueshifted) from the resonance line center while we work with quite small detunings. In conical emission, new frequencies are generated in the light-matter interactions. Analogously to the Fabry-Pérot interferometer diagnostics of the conical emission in [30] we have examined our scattered light. With a scanning Fabry-Pérot interferometer having a free spectral range of 2 GHz and a finesse of 200, we have not observed generation of new frequencies. We have performed the observations scanning the magnetic field while fixing the detuning of the laser frequency even far into the wings of the investigated resonance lines. As a conclusion we can state that, although the appearance of forward-scattered ring structures is quite similar to that of conical emission, the processes involved in creation of the forward-scattering rings are not as complicated as those leading to conical emission. However, in conical emission the cone structure depends also on the transverse beam profile. In forward scattering, and generally in level-crossing investigations information on atomic parameters can be derived from the magneto-optic spectra. It has been shown in this work that the spectra are sensitive to the laser-beam transverse profile—the parameter which is often ignored in these investigations.

---

*Present address: Joint Institute for Laboratory Astrophysics, Boulder, Colorado 80309-0440.

[1] J. Opt. Soc. Am. B 7 (6) (1990), special issue on Transverse Effects in Nonlinear-Optical Systems.

[2] Z. Phys. D **18** (1991), special issue dedicated to Professor W. Hanle on the occasion of his 90th birthday.

[3] A. Corney, B. P. Kibble, and G. W. Series, Proc. R. Soc. London, Ser. A **293**, 70 (1966).

[4] A. V. Durrant and B. Landheer, J. Phys. B **4**, 1200 (1971).

[5] W. Gawlik, J. Kowalski, R. Neumann, and F. Träger, Phys. Lett. **48A**, 283 (1974).

[6] W. Gawlik, J. Kowalski, R. Neumann, and F. Träger, Opt. Commun. **12**, 400 (1974).

[7] S. Giraud-Cotton, V. P. Kaftandjian, and L. Klein, Phys. Lett. **88A**, 453 (1982).

[8] W. Gawlik, Phys. Lett. **89A**, 278 (1982).

[9] S. Giraud-Cotton, V. P. Kaftandjian, and L. Klein, Phys. Lett. **90A**, 393 (1982).

[10] S. Giraud-Cotton, V. P. Kaftandjian, and L. Klein, Phys. Rev. A **32**, 2223 (1985).

[11] I. O. G. Davies, P. E. G. Baird, and J. L. Nicol, J. Phys. B **20**, 5371 (1987).
[12] K. H. Drake, W. Lange, and J. Mlynek, Opt. Commun. **66**, 315 (1988).
[13] L. M. Barkov, D. A. Melik-Pashayev, and M. S. Zolotorev, Opt. Commun. **70**, 467 (1989).
[14] P. E. G. Baird, M. Irie, and T. D. Wolfenden, J. Phys. B **22**, 1733 (1989).
[15] A. Weis, J. Wurster, and S. I. Kanorsky, J. Opt. Soc. Am. B **10**, 716 (1993).
[16] S. I. Kanorsky, A. Weis, J. Wurster, and T. W. Hänsch, Phys. Rev. A **47**, 1220 (1993).
[17] P. Jungner, T. Fellman, B. Ståhlberg, and M. Lindberg, Opt. Commun. **73**, 3842 (1989).
[18] B. Ståhlberg, P. Jungner, T. Fellman, and Å. Lindberg, Appl. Phys. B **50**, 547 (1990).
[19] B. Ståhlberg, P. Jungner, and T. Fellman, J. Phys. B **23**, L279 (1990).
[20] J. Zakrzewski and T. Dohnalik, J. Phys. B **16**, 2119 (1983).
[21] F. Schuller, M. J. D. MacPherson, and D. N. Stacey, Opt. Commun. **71**, 61 (1989).
[22] W. Gawlik and G. W. Series, in *Laser Spectroscopy,* edited by H. Walther and K. W. Rothe (Springer, Berlin, 1979), Vol. 4, pp. 210–221.
[23] K. Arnett, S. J. Smith, R. E. Ryan, T. Bergeman, H. Metcalf, M. W. Hamilton, and J. R. Brandenburg, Phys. Rev. A **41**, 2580 (1990).
[24] R. E. Ryan and T. H. Bergeman, Phys. Rev. A **43**, 6142 (1991).
[25] B. Ståhlberg, M. Lindberg, and P. Jungner, J. Phys. B **18**, 627 (1985).
[26] P. Jungner, B. Ståhlberg, and M. Lindberg, Phys. Scr. **38**, 550 (1988).
[27] S. Stenholm, *Foundations of Laser Spectroscopy* (Wiley, New York, 1984).
[28] B. Ståhlberg, P. Jungner, and T. Fellman, Appl. Spectrosc. **43**, 654 (1989).
[29] E. Konz, T. Kraft, and H.-G. Rubahn, Appl. Opt. **31**, 4995 (1992).
[30] J. F. Valley, G. Khitrova, H. M. Gibbs, J. W. Grantham, and Xu Jiajin, Phys. Rev. Lett. **64**, 2362 (1990).
[31] L. You, J. Mostowski, J. Cooper, and R. Shuker, Phys. Rev. A **44**, 6998 (1991).
[32] W. Chalupczak, W. Gawlik, J. Zachorowski, and D. Gawlik, in *Laser Spectroscopy,* edited by M. Ducloy, E. Giacobino, and G. Camy (World Scientific, Singapore, 1991), Vol. 10, pp. 314 and 315.
[33] L. You, J. Mostowski, and J. Cooper, Phys. Rev. A **46**, 2903 (1992); **46**, 2925 (1992).